https://doi.org/10.2352/EI.2022.34.15.COLOR-141

Camera Response Function Assessment in Multispectral HDR Imaging

Majid Ansari-Asl, Jean-Baptiste Thomas, and Jon Yngve Hardeberg; Norwegian University of Science and Technology; Gjøvik, Norway.

Abstract

Multispectral imaging techniques improve the accuracy of spectral reconstruction as well as color measurement in image-based data capture systems compared to the conventional RGB cameras. On the other hand, high dynamic range imaging provides recording a higher range of scene radiance values when the dynamic range of the camera does not cover values between the minimum and maximum radiances of the scene. In high dynamic range imaging, camera response function plays a crucial role in the irradiance map reconstruction. It could be either absolutely measured by laboratory equipment or relatively estimated through a set of images with different exposure times. In this work, camera response function assessment has been addressed for a filter wheel multispectral camera. Both measurement and estimation methods are investigated through experiments and results are compared to the ground truth data. The results showed high dynamic range imaging with measured absolute camera response function has two benefits: it measures radiance in the same scale and physical units, and outperformed in terms of the precision of reflectance measurement.

Introduction

Advances in technology allows study and production of materials with complex visual appearance attributes. These materials have found a lot of applications in various industries from interior design and car paintings to cosmetics and fashion to packaging and print technologies. [1] At the same time, scientific works have been done to propose models to fully characterize the appearance of such materials. To this aim, bidirectional reflectance distribution functions (BRDFs) is an accepted model for homogenous surfaces that currently can be measured properly. Image-based methods exploit cameras to capture BRDF of all the adjacent points over a surface which is not homogenous in appearance, i.e., spatially varying BRDF (svBRDF). Although cameras provide high resolution and faster data recording, they lack spectral capabilities and enough dynamic range.

In metrological and specifically BRDF measurement setups, precision of data capture is significantly important. However, most of the materials show specularity and speckle properties and have a dynamic range higher than dynamic range of the cameras. Therefore, faithful data capture in image-based BRDF systems needs high dynamic range imaging (HDRI). In HDRI software methods, multiple images with different exposure times are merged into an image with a higher dynamic range. On the other hand, multispectral imaging (MSI) enhances spectral reconstruction and color accuracy by recording the reflected radiance in several spectral bands and improves spectral reflectance measurement consequently.

There are three main elements in HDRI: camera response function (CRF), weight function, and multiple images with different exposure times. Most HDRI methods differ in the way they calculate CRF and therefore its assessment method affects the accuracy of the whole process. In this paper, the importance of CRF assessment method in multispectral HDRI is investigated in both radiance map reconstruction and reflectance measurements. In addition, the precision of results when CRF is measured/estimated for each filter separately is inquired, and results are evaluated by ground truth data captured by standard equipment.

Related Works

CRF measurement

In general, CRF measurement methods can be divided into two main groups: CRF measurement and CRF estimation. From another point of view, CRFs can be divided into absolute and relative functions. In spite to relative CRFs, in absolute CRFs the scales and physical units are preserved, and the exact irradiance could be retrieved from digital counts (camera responses). Therefore, the output of both CRF measurement and estimation methods can be either absolute or relative CRF function depending on the method.

While ISO 14524 describes a standard method for the measurement of absolute opto-electronic conversion functions of imaging systems including CRF by means of a specific test chart [2], in a similar approach Martinez et al. [3] used a classic ColorChecker (CC24) to measure absolute CRF. In another work, Guarnera et al. [4] exploited a projector to measure opto-electronic conversion transform. Brauers et al. [5] used an integrating sphere and a precise optical setup to measure relative CRF. On the other hand, many methods have been proposed to estimate CRF from a set of images taken from a scene with proper bracketing. The most successful works could be mentioned as methods proposed by Mann and Picard [6], Debevec and Malik [7], Mitsunaga and Nayar [8], and Robertson et al [9].

Multispectral HDRI

In the literature, some works have addressed HDRI for multispectral cameras. Brauers et al. [5] proposed a method to retrieve reflectance from HDR multispectral cameras. They have used a method to measure relative CRF. Lapray et al. [10] proposed HDRI for spectral filter array and estimated relative CRF. They have evaluated their method qualitatively and quantitatively but without ground truth data. Martinez et al. [3] used HDRI with measured absolute CRF for both LCTF camera and a filter wheel camera but they only removed filters, measured response function of the sensor, and used the same CRF in HDRI for all the spectral channels.

Theoretical Background

Reflectance Measurement in svBRDF

In BRDF, reflectance is defined as the ratio of reflected radiance by the incident irradiance in unit of sr^{-1}. As spatially varying BRDF is following the same definition and just adds spatial information to the BRDF, the definition of reflectance remains the same. Therefore, in image-based svBRDF and similarly bidirectional texture function (BTF) capture devices the reflectance is defined as follows: [11] [12]

$$\mathrm{P}_{x,\lambda} = \frac{L_{x,\lambda}}{E_{x,\lambda}} = \frac{g_{\lambda}^{-1}(I_{x,\lambda} - D_{x,\lambda})a_{\lambda}}{g_{\lambda}^{-1}(W_{x,\lambda} - D_{x,\lambda})\pi} \tag{1}$$

where $\mathrm{P}_{x,\lambda}$ is the reflectance in location x and wavelength λ. L and E are reflected radiance and incident irradiance respectively. The most important factors in this formula to be captured are $I_{x,\lambda}$, $D_{x,\lambda}$, and $W_{x,\lambda}$ representing image of the scene, dark noise image (just with turned off light source), and the image from a standard white reference, respectively. g_{λ}^{-1} indicates the inverse of camera response function and a_{λ} denotes the known spectral albedo of the standard white reference. For further details keen reader is referred to [12].

High Dynamic Range Imaging

The conventional cameras are usually limited in capturing scenes that contain contents with various amounts of radiances from very dark to very light. This is because of the low dynamic range of the camera. Figure 1 shows the CRF of a same camera used in this project. This camera is able to capture around 2.5 orders of magnitude while the dynamic range of the real-world objects is beyond this amount. In order to solve this problem, HDRI has been proposed and addressed in a lot of works in the literature. [13] and [14] cover HDRI comprehensively.

In general, two approaches are proposed for HDRI: software methods and hardware methods. In this work, the focus is on software methods. The concept of HDRI software methods is illustrated in Figure 2. Although the dynamic range of a given camera cannot be changed but by changing some settings including exposure time and aperture size, the minimum and maximum values of its dynamic range could be controlled. Figure 2 shows that by capturing multiple images with different exposure times and merging them together, a higher dynamic range could be reached.

Figure 2 illustrates the workflow of HDRI. Multiple low dynamic range (LDR) images are merged using Equation (2) and the HDR irradiance map is constructed. There are three main elements in this equation: g as camera response function (CRF) which defines the relation between the radiance reaching the camera and camera response digital counts, ω as weight function, and ρ multiple camera responses for different exposure times. Most of the different HDRI methods differ in the way they calculate CRF.

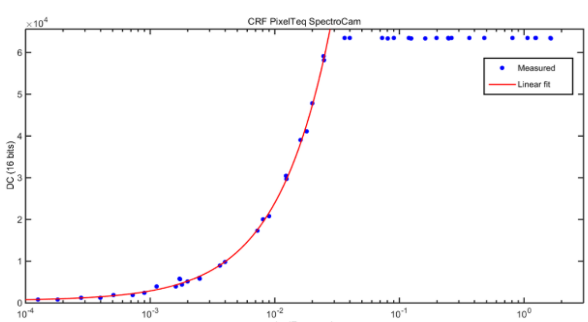

Figure 1 Camera Response Function (CRF) of Pixelteq SpectroCam. [3]

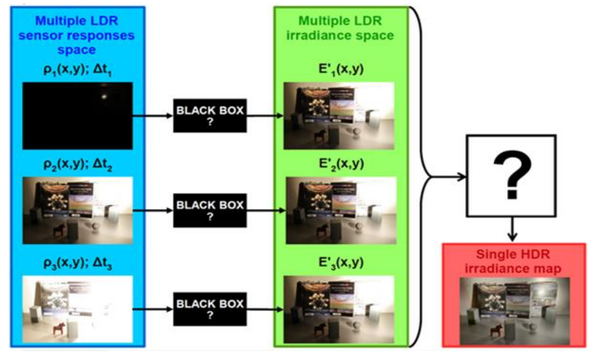

Figure 2 HDR imaging [3]. The LDR input images (left) taken with different exposure times are converted to LDR irradiance images by CRF and exposure times (middle), and then merged to construct HDR image.

$$E_k'(x,y) = \frac{\sum_{n=1}^{N} \omega(\rho_{nk}(x,y)) \frac{g^{-1}\rho_{nk}(x,y)}{\Delta t_n}}{\sum_{n=1}^{N} \omega(\rho_{nk}(x,y))} \tag{2}$$

Methodology

In this paper, CRF of Pixelteq SpectroCam multispectral camera with 6 filters is assessed with two methods: measurement and estimation. Afterwards, reflectance from the HDRI radiance maps are calculated and compared with reflectance values measured by a Konika Minolta CS2000 telespectroradiometer (TSR) as ground truth. Figure 3 shows the schematic of the work. It is clarified that, here, by spectral radiance and reflectance, it refers to the values of these measurands corresponding to the six wideband spectral filters used in this study.

Absolute CRF measurement:

Following [3], a CC24 is placed under a D65 simulator illumination source and the reflected spectral radiance from 24 patches are measured by TSR as ground truth. Then, the measured spectral radiances are multiplied by the ideal bandpass filters corresponding to the transmittance of the multispectral camera filters and the integral of multiplication output is calculated. These values give the total radiance reaching the camera for the given filters. These values are then multiplied by the corresponding camera exposure times and results are called pseudo-exposure. The camera filter transmittances and corresponding ideal bandpass filters are shown in Figure 4.

Afterwards, TSR is replaced with the multispectral camera and the CC24 is captured under the same illumination and imaging geometry with multiple exposure times. Subsequently, camera responses of 24 patches are calculated using taking average from a number of pixels approximately corresponding to the same area seen by the TSR. Finally, CRF is reconstructed from plotting corresponding pseudo-exposures and digital counts calculated from camera responses of 24 patches. In the end, a linear regression is done on the linear part of the extracted curve and considered as the measured absolute CRF.

Relative CRF estimation:

In this work, the relative CRF is estimated using Debevec and Malik's method as the most common method used in the literature. [7] In order to use this method to estimate CRF, a scene with high dynamic range content is to be captured by camera with multiple exposure times. The bracketing usually starts from exposure times that the image consists of under-exposed values to exposure times

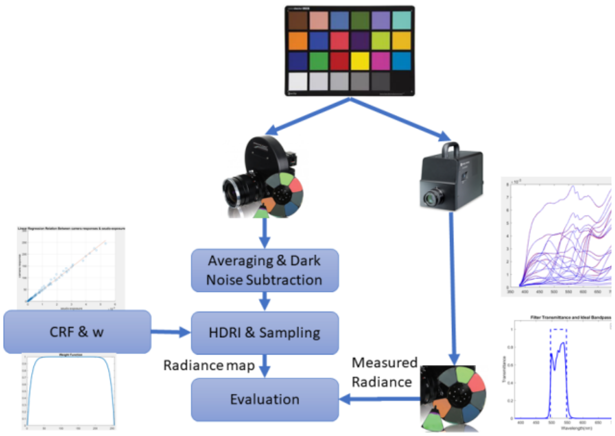

Figure 3 Schematic of this wok: measured reflected radiances from Colorchecker are passed through ideal filter are used as the ground truth data. Radiance maps are constructed by HDRI using measured/estimated CRF and camera responses after averaging and denoising.

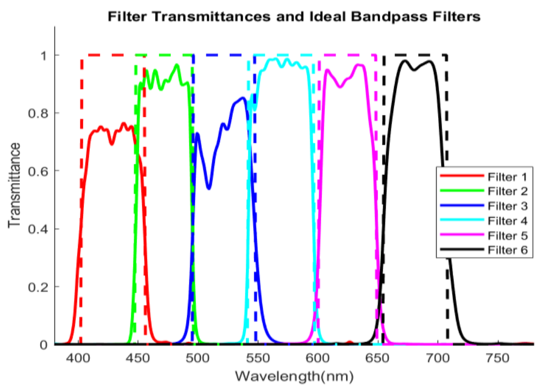

Figure 4 Filter Transmittances and Ideal Bandpass Filters.

with some image areas saturated. In this method, CRF is estimated through minimizing the following quadratic objective function:

$$f = \sum_{i=1}^{N} \sum_{j=1}^{P} \{\omega(Z_{i,j})[g(Z_{i,j}) - \ln E_i - \ln \Delta t_j]\}^2 + \gamma \sum_{z=Z_{min}+1}^{Z_{max}-1} [\omega(z) g''(z)]^2 \quad (3)$$

where $Z_{i,j}$ is pixel value in location i and corresponding to the exposure Δt_j, E_i irradiance in pixel location i, and g is the CRF. As pixel values closer to Z_{min} and Z_{max} might be poorly fitted by $g(z)$, a weighting function, $\omega(z)$, is introduced into the equation to guarantee the smoothness of CRF. Although a simple hat function as a reasonable choice is used in the original work, in this work both simple and broad hat functions are tested, and results of broad hat function is used in the next stages as results were almost identical.

Experiments

A Pixelteq SpectroCam filter wheel multispectral camera is used in this work. It has 8 different spectral bands. Six of those cover visible range, the first one in UV and the last one to cover near infrared. In addition, a Konika Minolta CS2000 telespectroradiometer (TSR) as the ground truth device and a XRite Digital ColorChecker SG (CCSG) which includes 24

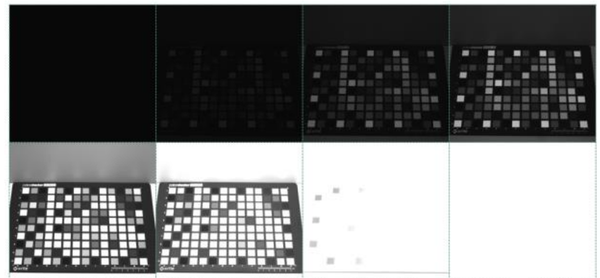

Figure 5 Some of average LDR images used for CRF measurement of 4th filter(570nm).

patches of CC24 as well are exploited. Macbeth SpectraLight III lightbooth has been used as the main light source but other extra light sources are also exploited when HDR scene was required.

Data capture for absolute CRF measurement

The TSR measurements and multiple capture of CCSG with different camera exposure times are required to construct absolute measurements. The CCSG is placed in the light booth and the spectral radiances of 24 patches corresponding to CC24 are measured with TSR before and after data capture to ensure the stability of light source during experiments.

The TSR is then replaced by the Pixelteq SpectroCam filter wheel camera and the multispectral images are taken with 11 different exposure times. For each exposure time, data capture and dark image with installed camera cap are repeated 10 times. Figure 5 shows average images of 10 iterations for the 4th filter (570 nm). In this image, each image for a given exposure time is presented next to its corresponding dark noise image. Exposure times are 0.064, 0.1, 0.5, 1, 5, 10, 50, 100, 500, 1000, and 2000 all in mili-seconds (ms).

Data capture for CRF estimation using Debevec and Malik method

Image acquisition for CRF estimation using Debevec and Malik method needs a scene with high dynamic range content to be captured. Therefore, a scene in a dark room was created which contains a light booth as well as two extra light sources illuminating inside the light booth to provide a high dynamic range scene. Then, the scene is captured using the SpectroCam filter wheel camera with 32 different exposure times: 1, 2, 3, 4, 5, 6, 7, 8, 9, 10, 20, 30, 40, 50, 60, 70, 80, 90, 100, 200, 300, 400, 500, 600, 700, 800, 900, 1000, 1250, 1500, 1740, and 2000 all in ms. The 32 photos each channel is chosen arbitrarily (size of the dataset collected) while it is reported that higher number of images used in Debevec and Malik's method would increase the noise sensitivity. [7] However, since this method is a relative CRF estimation, ground truth data capture by TSR is not required. Some sample images as inputs for this method are shown in Figure 6 for the 4th filter (570 nm).

The linear part of CRFs measured and estimated, after linear fitting and expanding to the whole digital counts range, are illustrated in Figure 7. In the measured CRF, (Figure 7-a), different channels have different behaviors because not only the corresponding filters have different transmittance shapes, but also spectral sensor responsivity has different characteristic in different channels. This is not the case for the estimation method as it mainly affects the slope and in relative measurement it does not matter too much.

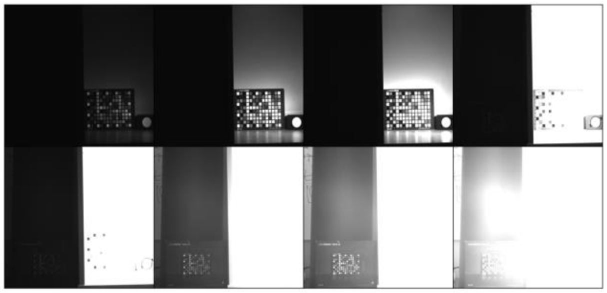

Figure 6 Some of LDR images used for CRF estimation by Debevec's method; 4th filter(570nm).

Radiance map reconstruction and reflectance calculation

A subset of images taken for absolute CRF measurement consist of six exposure times: 1, 5, 10, 50, 100, 500 ms are selected for radiance map reconstruction and reflectance calculation which are reasonable exposures avoiding too much under and over exposures. The same images are used as input data for both HDRI with relative CRF estimation and absolute CRF measurement methods. The reconstruction error analysis, error between HDRI output and ground truth, has been done using root mean square error (RMSE) metric defined as:

$$RMSE = \sqrt{\frac{\sum_{k=1}^{N}(P_k - \hat{P}_k)^2}{N}} \quad (4)$$

that P_k indicates measured radiance or reflectance in k[th] channel, N represents number of channels, and $\hat{P}_k$ is the corresponding ground truth data.

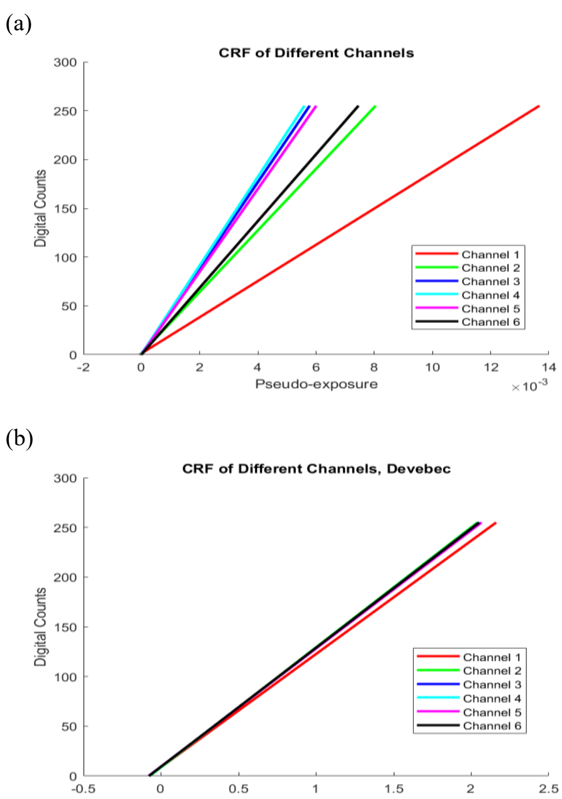

Figure 7 Camera response function of different channels: (a) measurement (b)estimation using Debevec method.

Results and Discussion

Radiance map reconstruction

The radiance maps are reconstructed after CRF measurement and estimation. Since ground truth data is a spot measurement, the same areas seen by the TSR are averaged from radiance map images corresponding to 24 patches of CC24 and used for data analysis. The spectral radiances, with six spectral channels, calculated from HDR images reconstructed using CRF measurement method are compared to ground truth data. Figure 8 shows the spectral radiance of the first 6 patches, and RMSEs are represented in Figure 9 for all the 24 patches. The average of RMSE is 0.0071 $\frac{W}{m^2.Sr}$ with a standard deviation of 0.0054. Figure 9 shows that the measurement error for patches with higher luminance is greater than darker patches and the 19[th] patch with the highest luminance has the largest error value among others. This analysis implies that the performance of HDRI with the CRF measurement method is acceptable with regards to radiance measurement and the outputs are in the same scale and physical units as standard measurement systems while HDRI with estimation method outputs relative radiances, and it does not have meaning to compare its results with the ground truth.

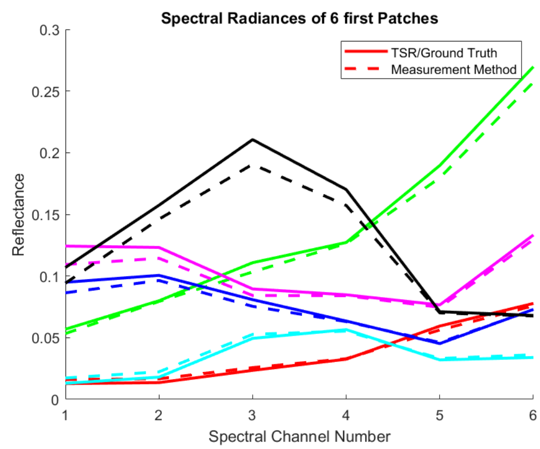

Figure 8 Spectral radiances of 6 first patches.

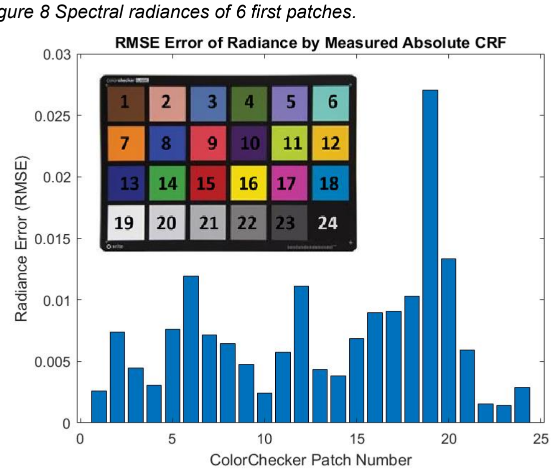

Figure 9 Spectral errors of radiance measurement by camera and HDRI when CRF is absolutely measured.

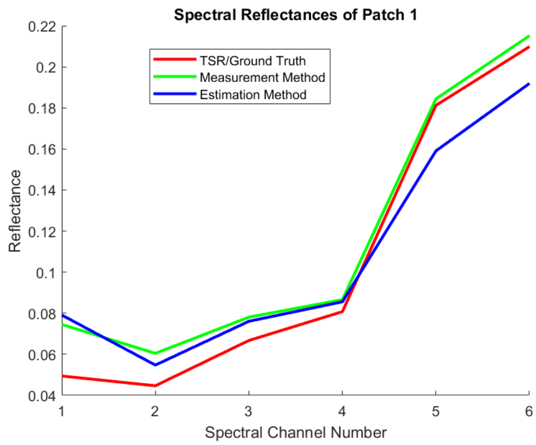

Figure 10 Spectral reflectance of the 1st patch.

TABLE 1 REFLECTANCE MEASUREMENT ERROR.

		RMSE Error	
		Mean	Standard Deviation
Reflectance of 24 Patches	Measurement	0.0185	0.0080
	Estimation	0.0313	0.0130
Reflectance of 6 channels	Measurement	0.0188	0.0079
	Estimation	0.0314	0.0137

Spectral reflectance analysis

In a further step, the white patch of the CC24, patch number 19, is considered as the reference white and reflectances are computed by the ratio of patch radiances to the radiance of this patch. As an example, Figure 10 illustrates reflectance of the first patch measured by two methods as well as TSR. The RMSEs are calculated with two approaches: in the first approach, the spectral reflectances, 6 channels, are obtained for the 24 patches and compared to the ground truth data. Table 1 summarizes the accuracy of reflectance measurement by two methods. The error is reported 0.0185 and 0.0313 as average error and 0.0080 and 0.0130 as standard deviation for CRF measurement and CRF estimation methods respectively, and obviously the measurement outperformed the estimation method as its average error is almost half of the other method.

In the second approach, the RMSE error of each spectral band is analyzed separately to evaluate the efficiency of different methods in reflectance measurement in different spectral channels. Table 1 indicates that as expected, measurement method has a better performance in channel-wise analysis as well since it has half average RMSE of the other method. Figure 11 presents bar plot of reflectance measurement errors. It is obvious that the HDRI with measured absolute CRF has outperformed the other method in all the spectral channels and all the CC24 patches. In Figure 11-(a), the error for patch number 19 equals to zero because it had been used as the reference white in the experiment. Figure 12 represents the errors in boxplot to provide a better visualization of the distribution of reflectance measurement errors.

Conclusions and Future Works

In this paper, the evaluation of multispectral HDRI is addressed with regards to different CRF assessment methods. Two different methods of CRF assessment have been implemented: in the first method absolute CRF is measured by means of reflective color charts and in the second method relative CRF is estimated through a well-known estimation method. HDRI is exploited to construct radiance map utilizing both CRFs and results are evaluated by comparing to the TSR measurements as ground truth. Radiances measured by camera using HDRI and measured absolute CRF matches with ground truth, but a significant mismatch is reported for HDRI using estimated relative CRF due to its relative behavior. However, reflectances are also calculated and results showed the reflectance measurement accuracy outperformed by the absolute CRF measurement method. This work is relevant since precision of HDRI is crucial in metrological measurements such as svBRDF devices. Although specularities in material are of higher dynamic range than the tested scene but there is little risk that the conclusion would differ. In addition, this comparison helps industries to opt a proper method between CRF estimation and cumbersome measurement methods in their products.

As for directions for further work, experiments with larger data capture, and including spectral reconstruction are suggested. Using HDR scenes in the final evaluation and cameras with different filter transmittances would show the importance of this investigation better than LDR scenes.

(a)

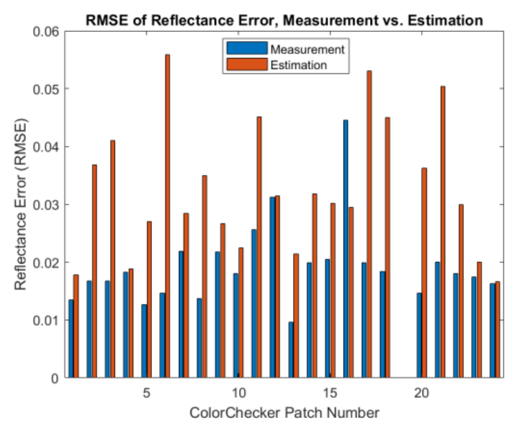

(b)

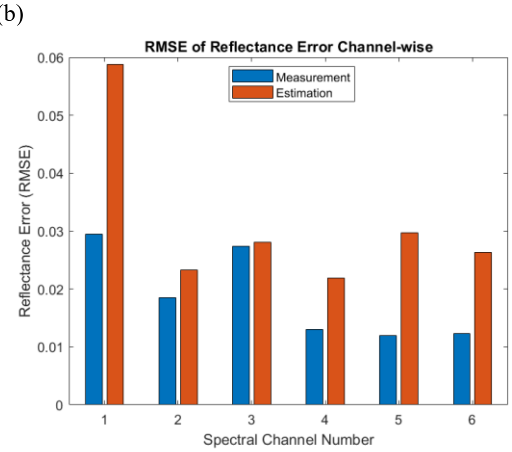

Figure 11 Reflectance measurement error: (a) 24 CC24 patches (B) six spectral channels.

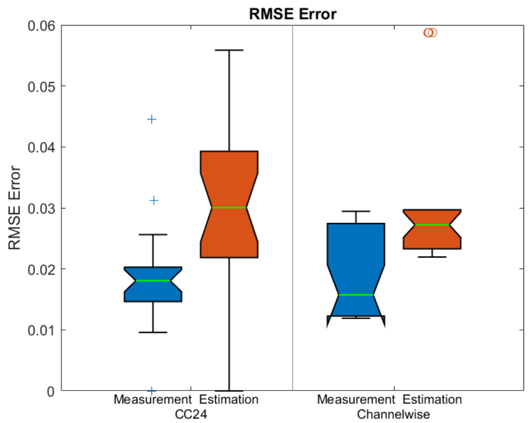

Figure 12 The distribution of RMSE reflectance errors.

ACKNOWLEDGMENT

This project has received funding from the ApPEARS-Appearance Printing European Advanced Printing School European Union's Horizon 2020 research and innovation programme under the Marie Skłodowska-Curie grant agreement No. 814158.

References

[1] G. Obein, "The measurement of appearance," in *New Frontiers for Metrology: From Biology and Chemistry to Quantum and Data Science*, IOS Press, 2021, pp. 175-186.

[2] ISO 14524, *Photography-Electronic Still Picture Cameras--Methods for Measuring Opto-Electronic Conversion Functions (OECFs),* Switzerland: International Organization for Standardization Geneva, 2009.

[3] M. A. Martínez, *Multispectral High Dynamic Range Polarimetric Imaging applied to scene segmentation and object classification,* Granada: Ph.D. dissertation, Universidad de Granada, 2017.

[4] G. C. Guarnera, S. Bianco and R. Schettini, "Turning a Digital Camera into an Absolute 2D Tele-Colorimeter," *Computer Graphics Forum,* vol. 38, no. 1, pp. 73-86, 2019.

[5] J. Brauers, S. Nils, A. A. Bell and T. Aach, "Multispectral high dynamic range imaging," in *Color Imaging XIII: processing, hardcopy, and applications*, San Jose, CA, USA, 2008.

[6] S. Mann and R. Picard, "On Being "Undigital" With Digital Cameras: Extending dynamic Range by Combining Differently Exposed Pictures," *MIT Media Lab Perceptual,* vol. 1, p. 2, 1994.

[7] P. E. Debevec and J. Malik, "Recovering high dynamic range radiance maps from photographs," in *ACM SIGGRAPH 2008 classes*, Los Angeles, USA, 2008.

[8] T. Mitsunaga and S. K. Nayar, "Radiometric self calibration," in *Computer Vision and Pattern Recognition*, 1999.

[9] M. A. Robertson, S. Borman and R. L. Stevenson, "Estimation-theoretic approach to dynamic range enhancement using multiple exposures," *J. Electronic Imaging,* vol. 36, no. 2, pp. 162-170, 1992.

[10] P.-J. Lapray, J.-B. Thomas and P. Gouton, "High dynamic range spectral imaging pipeline for multispectral filter array cameras," *Sensors,* vol. 17, no. 6, p. 1281, 2017.

[11] V. Havran, J. Hošek, Š. Němcová, J. Čáp and J. Bittner, "Lightdrum—Portable light stage for accurate BTF measurement on site," *Sensors,* vol. 17, no. 3, p. 423, 2017.

[12] C. Schwartz, R. Sarlette, M. Weinmann, M. Rump and R. Klein, "Design and implementation of practical bidirectional texture function measurement devices focusing on the developments at the University of Bonn," *Sensors,* vol. 14, no. 5, pp. 7753-7819, 2014.

[13] E. Reinhard, W. Heidrich, P. Debevec, S. Pattanaik, G. Ward and K. Myszkowski, High dynamic range imaging: acquisition, display, and image-based lighting, Morgan Kaufmann, 2010.

[14] E. Reinhard, E. A. Khan, A. O. Akyuz and G. Johnson, Color imaging: fundamentals and applications, CRC Press, 2008.